Applied Physics Letters

Band offset determination for amorphous Al_2O_3 deposited on bulk AlN and atomic-layer epitaxial AlN on sapphire

Cite as: Appl. Phys. Lett. **117**, 182103 (2020); https://doi.org/10.1063/5.0025835
Submitted: 18 August 2020 . Accepted: 26 October 2020 . Published Online: 05 November 2020

Chaker Fares, Fan Ren, Marko J. Tadjer, Jeffrey Woodward, Michael A. Mastro, Boris N. Feigelson, Charles R. Eddy, and S. J. Pearton

Applied Physics Letters ARTICLE scitation.org/journal/apl

Band offset determination for amorphous Al_2O_3 deposited on bulk AlN and atomic-layer epitaxial AlN on sapphire

Cite as: Appl. Phys. Lett. **117**, 182103 (2020); doi: 10.1063/5.0025835
Submitted: 18 August 2020 · Accepted: 26 October 2020 ·
Published Online: 5 November 2020

Chaker Fares,[1] Fan Ren,[1] Marko J. Tadjer,[2,a)] Jeffrey Woodward,[3] Michael A. Mastro,[2] Boris N. Feigelson,[2] Charles R. Eddy, Jr.,[2] and S. J. Pearton[4]

AFFILIATIONS

[1]Department of Chemical Engineering, University of Florida, Gainesville, Florida 32611, USA
[2]Naval Research Laboratory, Washington, DC 20375, USA
[3]American Society for Engineering Education Postdoctoral Fellow, Residing at Naval Research Laboratory, Washington, DC 20375, USA
[4]Department of Materials Science and Engineering, University of Florida, Gainesville, Florida 32611, USA

Note: This paper is part of the Special Topic on Ultrawide Bandgap Semiconductors.
[a)]**Author to whom correspondence should be addressed:** marko.tadjer@nrl.navy.mil

ABSTRACT

Valence and conduction band offsets of atomic layer deposition (ALD) Al_2O_3 deposited on bulk AlN crystals were determined using x-ray photoelectron spectroscopy to be $\Delta E_V = 0.75$ eV and $\Delta E_C = -1.45$ eV, with a measured energy gap of the Al_2O_3 film of 6.9 eV. In addition, crystalline AlN deposited by atomic layer epitaxy on sapphire was evaluated, resulting in a valence band offset of $\Delta E_V = -0.75$ eV and a conduction band offset of $\Delta E_C = 3.25$ eV due to the wider bandgap of the crystalline Al_2O_3 substrate compared to amorphous ALD Al_2O_3. Both heterojunctions exhibited type-II behavior and similar valence band offsets.

The past several years have witnessed the emergence of a number of wide and ultra-wide bandgap (UWBG) semiconductors for electronic device applications.[1] Gallium-based compounds such as gallium nitride (GaN), which has found widespread commercial application, and gallium oxide (Ga_2O_3), which has only recently gathered widespread interest as a device material, both offer advantageous properties such as a high critical field.[2,3] Additionally, the capability to incorporate Al and form ternary alloys has further extended the capabilities of these material systems into heteroepitaxial device structures such as AlGaN/GaN and $(AlGa)_2O_3/Ga_2O_3$ heterostructure field effect transistors (HFETs).[4,5] At high Al concentrations, AlN and Al_2O_3 are the widest bandgap III-Nitride and III-Oxide components of these material systems.[6–9] In particular, AlN technology has demonstrated native substrates, high quality epitaxial growth, and possibility for relatively shallow n-type donors.[1] While AlN/GaN HFETs have been developed for some time, the first AlN channel transistor with implanted source/drain was only recently demonstrated.[10–12] Most recently, improved understanding of Si doping in AlN has renewed interest in this UWBG material for electronic devices for high breakdown voltage, high power applications.[13–17] As a result, a number of fundamental electronic experiments, such as the presently reported band diagrams, are needed for UWBG materials such as AlN, as has been the case with recent band diagram investigations for other promising materials such as β-Ga_2O_3.[2]

One of the fundamental methods of understanding the electronic properties of heterostructures between different materials is the construction of their band diagram. In the literature, band offset reports of oxide-semiconductor and semiconductor-semiconductor heterostructures abound as device technology has advanced over the years. Particularly for the III-N and III-O systems, a large body of literature exists for band offsets as different gate dielectrics are explored: SiO_2, Al_2O_3, and HfO_2 being among the most popular. Ternary nitride alloys with Al and their band structures have been reported.[18] Band offsets between the binary III-O and III-N semiconductor heterojunctions have also been recently explored. The band alignments of AlN, GaN, and InN heterojunctions to Ga_2O_3, as well as GaN-Al_2O_3 and InN-Al_2O_3, are all known.[19–23] The InN-In_2O_3 heterojunction, which is relevant for thin-film transistor technology, has been studied as

well.[24] This paper aims to bridge the current gap in band offset knowledge between oxides and nitrides by characterizing the AlN-Al_2O_3 heterojunction using deposited films of Al_2O_3 and AlN on single-crystalline substrates of AlN and Al_2O_3, respectively.

We deposited amorphous Al_2O_3 on bulk single-crystalline AlN substrates using atomic layer deposition. In addition, atomic-layer deposited epitaxial AlN has been grown on substrates of a-plane Al_2O_3. Al_2O_3 was deposited by atomic layer deposition (ALD) on single-crystalline AlN substrates obtained commercially. These samples are, henceforth, referred to as Al_2O_3/AlN. Both thick (200 nm) and thin (1.5 nm) layers of the Al_2O_3 dielectric were deposited to measure both the bandgaps and core levels. For pre-deposition substrate cleaning, the following rinse sequence was employed: acetone, isopropyl alcohol (IPA), dry N_2, and finally ozone exposure for 15 min. ALD Al_2O_3 was deposited at 200 °C in a Cambridge Nano Fiji 200 using a trimethylaluminum source and a remote inductively coupled plasma (ICP) of O_2 at 300 W.[25,26]

The atomic layer epitaxial (ALE) AlN films on the a-place sapphire, henceforth referred to as AlN/Al_2O_3, were grown at 525 °C using a Veeco/Cambridge Nanotech (CNT) Fiji 200 and ultra-high purity (UHP) gases, with constant 100 and 30 sccm flows of Ar through the plasma source and precursor line, respectively.[9,27] Prior to AlN deposition, the Al_2O_3 substrates were cleaned by sonicating in sequential 5 min baths of acetone and isopropanol at 40 °C and a final bath in de-ionized water. The substrates were then dried in N_2, loaded into the reactor, and heated to growth temperature. An *in situ* cleaning process was performed immediately prior to growth. The *in situ* cleaning process consisted of subjecting the substrates to 10 cycles each of H_2 and N_2 plasma exposure at 300 W forward power, during which 75 (50) sccm H_2 (N_2) was flowed through the plasma source in addition to the Ar. Every cycle was 20 s in duration and was followed by a 10 s purge with only Ar flowing.

The AlN growth process consisted of 500 cycles of the following. First, the sample surface was saturated by a 60 ms pulse of trimethylaluminum. The chamber was then purged by the Ar flow for 8 s in order to remove excess precursor and reaction byproducts. Next, the precursor-terminated surface was exposed to a mixed N_2/H_2 plasma at 300 W forward power for 20 s, during which 75 sccm of N_2 and 10 sccm of H_2 were flowed through the plasma source in addition to the Ar. Finally, residual gases and reaction byproducts were removed by a second Ar purge, completing the cycle.

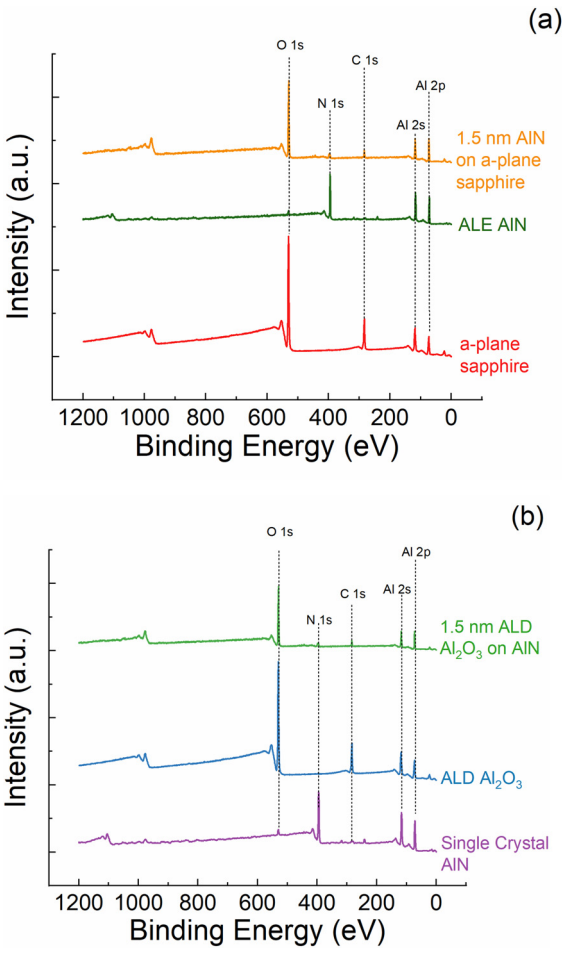

FIG. 1. XPS survey scans of (a) single crystal AlN, ALD Al_2O_3, and a heterostructure of Al_2O_3 on AlN and (b) a-plane sapphire, ALE AlN, and a heterostructure of AlN on sapphire. The intensity is in arbitrary units (a.u.).

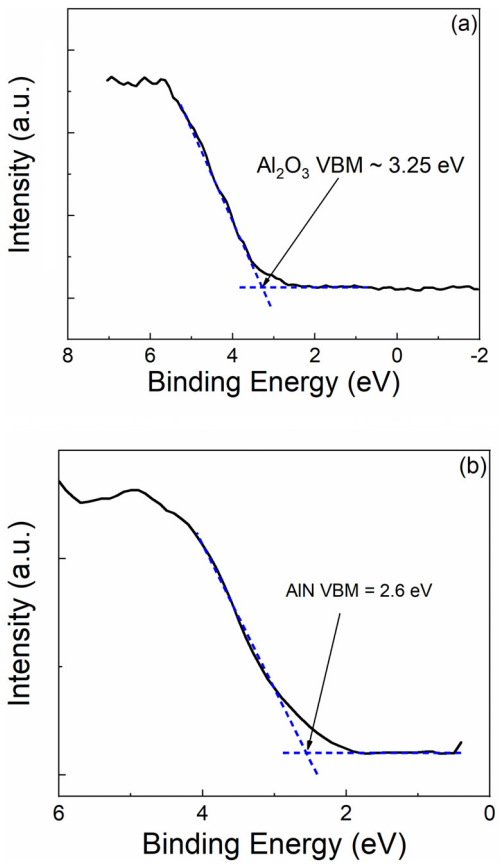

FIG. 2. XPS spectra of the valence band maxima (VBM) for (a) reference thick-film ALD Al_2O_3 and (b) thick-film ALE AlN. The intensity is in arbitrary units (a.u.).

After deposition, the Al_2O_3/AlN and AlN/Al_2O_3 samples were transferred into the chamber of an ULVAC PHI XPS system. A monochromatic, Al x-ray source with a power of 300 W and a dual beam charge neutralization system with simultaneous low-energy electron and ion means were used to perform the charge-compensated XPS measurement.[28] Charge correction was performed using the adventitious carbon (C–C) line in the C 1s spectra at 284.8 eV. All spectroscopic equipment and electron analyzers were grounded. Samples were electronically insulated from the chuck to avoid differential charging effects, which were not observed.[29] The bandgap of Al_2O_3 was measured using reflection electron energy loss spectroscopy (REELS) with a 1 kV electron beam and the hemispherical electron analyzer.[30]

The band offsets of the Al_2O_3/AlN and AlN/Al_2O_3 heterojunctions were measured with high precision using the XPS method developed by Kraut *et al.*[29] To obtain band offsets using this technique, the core energy levels and the valence band maxima of each material need to be measured first. For the Al_2O_3/AlN heterojunction, the valence band offset (VBO) is then given by

$$\Delta E_V = \left(E_{core}^{Al2O3} - E_{VBM}^{Al2O3}\right) - \left(E_{core}^{AlN} - E_{VBM}^{AlN}\right) - \left(E_{core}^{O1s} - E_{core}^{N1s}\right). \quad (1)$$

For the conduction band offset of the heterojunction, the bandgap of each constituent material needs to be known. The conduction band offset is thus given by

$$\Delta E_C = E_G^{Al2O3} - E_G^{AlN} - |\Delta E_V|. \quad (2)$$

Figure 1 shows the XPS scans of the two Al_2O_3 films and the bulk AlN reference. The signature Al 2p, N 1s, and O 1s peaks from the two materials expected to be present were readily observable. An O 1s peak was observable on the AlN substrate reference scan [Fig. 1(a)] but was greatly suppressed and was likely due to O impurities in the crystal. The N 1s peak showed the highest intensity in the AlN substrate and was suppressed as thin ALD Al_2O_3 was deposited. The N 1s peak was not observed from the sample with thick ALD Al_2O_3 on the AlN substrate. Nearly identical peaks were observable from the XPS scans of the ALE AlN films on a-plane sapphire, as shown in Fig. 1(b).

Figure 2 shows the measured valence band maxima (VBM) from the thick Al_2O_3 film [Fig. 2(a)] and the bulk AlN substrate [Fig. 2(b)] as 3.25 and 2.6 eV, respectively. Identical results (not shown) were obtained for the AlN/sapphire sample. This is particularly interesting

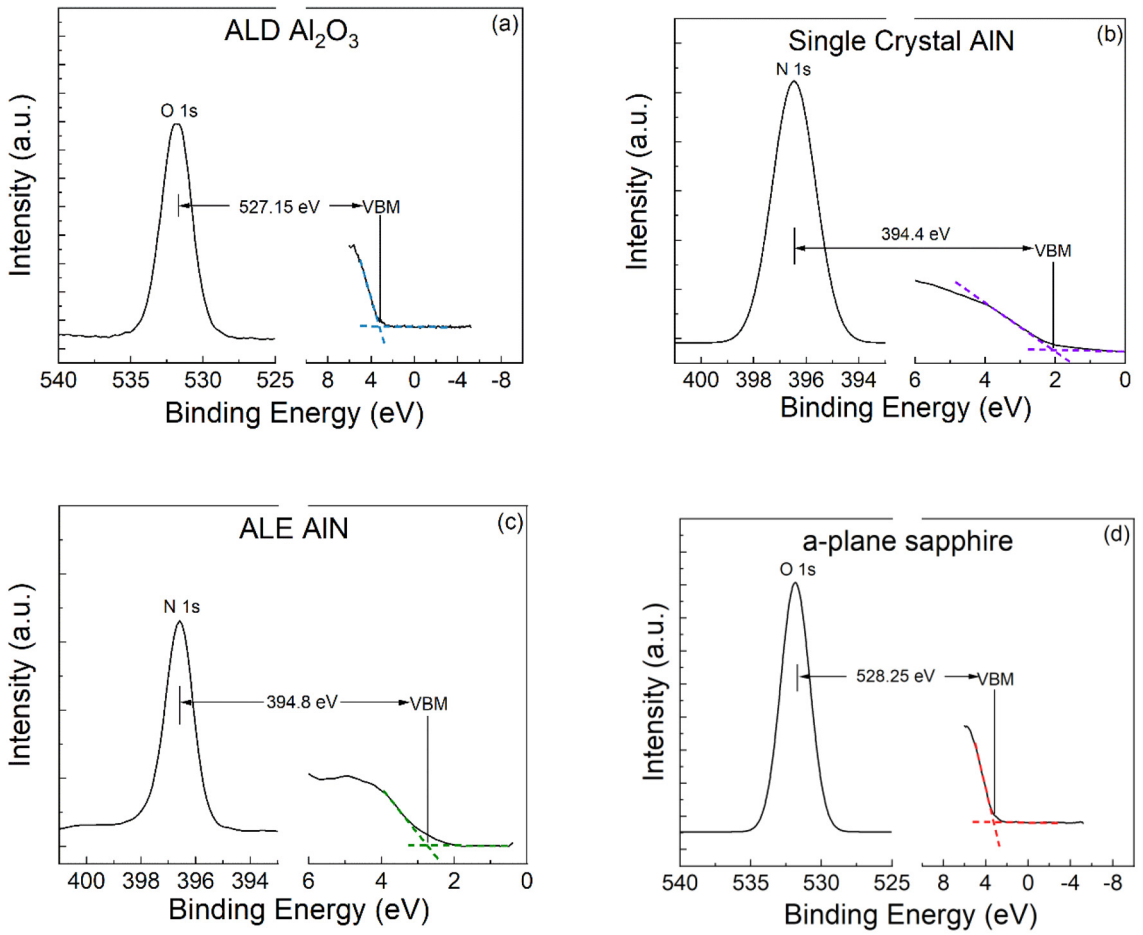

FIG. 3. High resolution XPS spectra for the vacuum-core delta regions of (a) reference thick film ALD Al_2O_3 and (b) reference single crystal AlN for the ALD Al_2O_3/AlN sample; (c) thick film ALE AlN and (d) reference Al_2O_3 for the ALE AlN/Al_2O_3 sample. The intensity is in arbitrary units (a.u.).

TABLE I. Summary of measured core levels (eV) for single crystal AlN, ALD Al_2O_3, and a heterostructure of ALD Al_2O_3 deposited on bulk AlN.

Single crystal AlN				ALD Al_2O_3				Thin ALD Al_2O_3 on single crystal AlN	
Core level	VBM	Core level peak	Core-VBM	Core level	VBM	Core level peak	Core—VBM	Δ Core level N1s—O1s	Valence band offset (VBO)
N1s	2.1	396.5	394.4	O1s	3.25	530.4	527.15	−133.5	0.75 ± 0.05

TABLE II. Summary of measured core levels (eV) for a-plane sapphire, ALE AlN, and a heterostructure of AlN on sapphire.

Reference Al_2O_3				Reference AlN				Thin AlN on Al_2O_3	
Core level	VBM	Core level peak	Core—VBM	Core level	VBM	Core level peak	Core—VBM	Δ Core level O1s—N1s	Valence band offset (VBO)
O1s	3.25	531.50	528.25	N1s	2.6	397.4	394.8	134.2	−0.75 ± 0.05

considering that amorphous ALD Al_2O_3 and a bulk sapphire crystal were compared in this work. In comparison to previous work, similar valence band maxima for amorphous and crystalline Al_2O_3 were also reported by Filatova and Konashuk[31] and Balzarotti and Bianconi.[32]

To obtain the energy difference between the VBM energies for each material and the core shell N 1s electrons for AlN and O 1s electrons for Al_2O_3, the previously measured VBM maxima are compared with core shell XPS data obtained from the 200 nm thick films. The energy difference spectra are shown in Fig. 3(a) for the ALD Al_2O_3, Fig. 3(b) for the bulk AlN substrate, Fig. 3(c) for the ALE AlN film, and Fig. 3(d) for the sapphire substrate. The energies measured from each comparison were 527.15 eV [Fig. 3(a)], 394.4 eV [Fig. 3(b)], 394.8 eV [Fig. 3(c)], and 528.25 eV [Fig. 3(d)], respectively. These results are summarized in the first two columns of Tables I and II.

To complete obtaining the experimental data required in Eq. (1), the energy difference between the same two core shell electron energies at the interface of the heterojunction was measured on samples of a 1.5 nm thick film on a bulk substrate. Figure 4(a) shows the core level difference from the 1.5 nm thick ALD Al_2O_3 film on the AlN substrate to be 133.5 eV. For the 1.5 nm ALE AlN film on sapphire, this energy difference was measured to be 134.2 eV, as shown in Fig. 4(b). Thus, according to Eq. (1), a VBO of $+0.75\pm0.05$ eV was calculated for the ALD Al_2O_3 on the bulk AlN sample, whereas a VBO of -0.75 ± 0.05 eV was calculated for the ALE AlN on the sapphire sample. These results are summarized in Tables I and II as well.

The REELS data for the amorphous ALD Al_2O_3 film are shown in Fig. 5, indicating a 6.9 eV bandgap. The bandgap of crystalline sapphire substrates has been reported in several works.[6,7] In this case, we assumed a bandgap of 8.7 eV for the a-Al_2O_3 substrate.[7,33] The difference in bandgap between amorphous and crystalline Al_2O_3 is due to their significant difference in density (4.0 g/cm^3 for α-Al_2O_3 and 3.1–3.3 g/cm^3 for amorphous phase Al_2O_3), which in turn results in a significant coordination difference.[34–39] The bandgap of ALE AlN has been reported previously to be 6.2 eV. The bandgap of bulk AlN was assumed to be 6.2 eV as well, as both materials are of crystalline nature.[9]

The resulting energy band diagrams are shown in Fig. 6, which illustrates how conduction band offsets are obtained from the valence

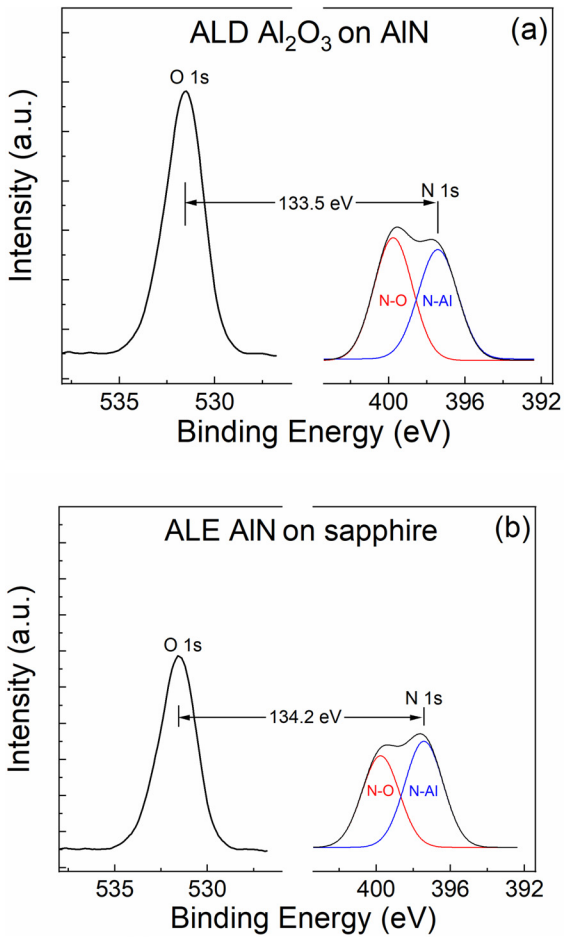

FIG. 4. High resolution XPS spectra for (a) 1.5 nm ALD Al_2O_3 on AlN and (b) 1.5 nm ALE AlN on Al_2O_3 (sapphire) core delta regions. The intensity is in arbitrary units (a.u.).

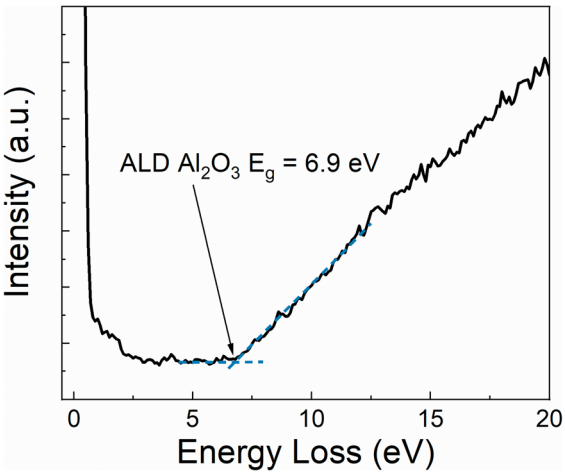

FIG. 5. Bandgap of the Al_2O_3 used in this study determined by RHEELS data. The intensity is in arbitrary units (a.u.).

band offset and the energy gap of the two constituent materials. Thus, the conduction band offset was calculated to be 1.45 eV based on the valence band offset of +0.75 eV for ALD Al_2O_3 on bulk AlN [Fig. 6(b)] and the energy gaps of 6.9 eV and 6.2 eV for ALD Al_2O_3 and bulk AlN, respectively, resulting in a type-II band diagram for the case of ALD amorphous Al_2O_3 deposited on a crystalline AlN substrate. For the ALE AlN on sapphire, type-II behavior was obtained as well with a conduction band offset of 3.25 eV, owing to the larger bandgap for the sapphire substrate [Fig. 6(a)]. In both cases, the experimentally obtained conduction band offsets were significantly higher than the values reported by Robertson and Falabretti.[39]

Obtaining the band offsets for this heterojunction has two important consequences. First, it shows that Al_2O_3 is a possible candidate dielectric for AlN electronic devices such as lateral AlN transistors.[10] Second, it lays the groundwork for future experiments into the band offsets for heterojunctions of ternary oxide alloys such as $(Al_xGa_{1-x})_2O_3$ to both binary and ternary nitrides. Similarly, our recent study of band offsets in the InN/Ga_2O_3 system had complemented the band offset reports for GaN/Ga_2O_3 and AlN/Ga_2O_3, allowing us to combine the data in order to estimate band offsets for the ternary nitride alloys to Ga_2O_3.[21] We note that band offset data for the In_2O_3/GaN and In_2O_3/AlN heterojunctions are still lacking in the literature, as well as bowing parameter data for the $(Al_xIn_{1-x})_2O_3$ ternary oxide alloy as phase segregation likely is a major issue when determining the fundamental crystal structure of this alloy.[40,41] Future work will thus focus on completing the characterization of band offsets along the ternary spectra of Al_2O_3, Ga_2O_3, AlN, GaN, In_2O_3, and InN.

The band offset of the Al_2O_3/AlN heterojunction has remained unexplored so far, as it has not been relevant for device applications. Understanding this heterostructure will pave the way for further experiments into oxide/nitride semiconductor integration. In previous studies of another potentially relevant heterojunction, InN-Ga_2O_3, it was proposed that knowledge of binary heterojunction band offsets could be used to calculate and predict band offsets for ternary heterojunctions.[21] This was done for the ternary nitride compounds AlGaN, AlInN, and InGaN with the binary compound Ga_2O_3. In that work, it was noted that in order to calculate the band offsets for ternary oxides to binary nitrides, knowledge of the Al_2O_3/AlN system is necessary. Furthermore, it was noted that eventually oxide and nitride semiconductor integration effort will be able to produce heterojunctions between ternary oxides and nitrides directly and proposed a set of simple equations to extrapolate their band offsets using the binary

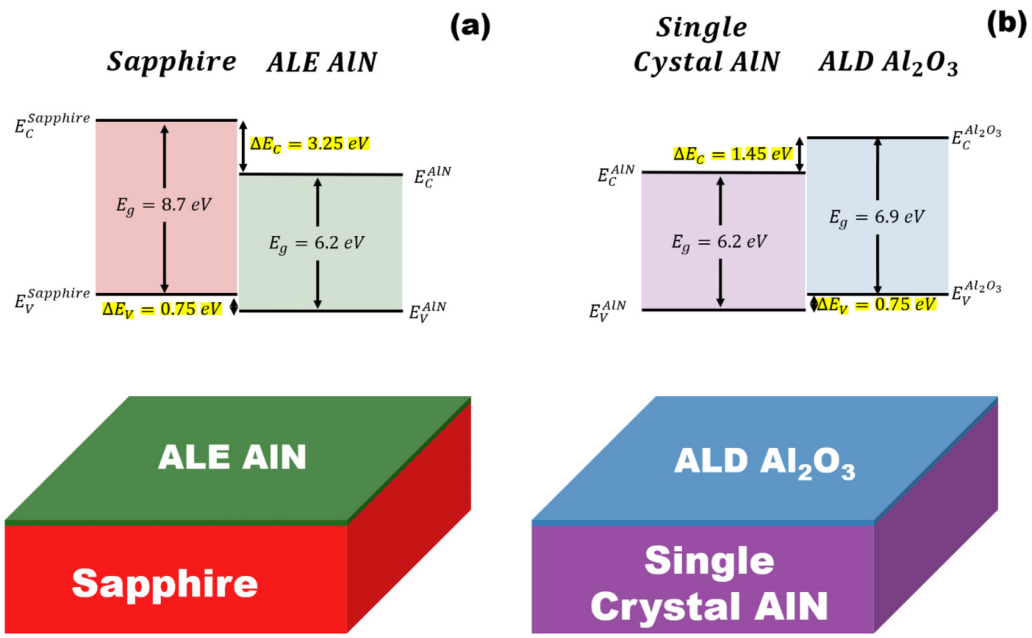

FIG. 6. Band diagrams for (a) ALD Al_2O_3 on bulk AlN and (b) ALE AlN on a-plane sapphire (a-Al_2O_3).

compounds' band offset data. The measurements presented in this work present the last missing binary oxide/nitride semiconductor band offset data before any further band offset studies of ternary oxide/nitride heterojunctions can be performed.

In summary, the band alignments of ALD Al_2O_3 on single crystal AlN and crystalline AlN on sapphire were measured. These are valuable in providing input to first-principles calculations of the band offsets for ternary oxide alloys such as $(Al_xGa_{1-x})_2O_3$ and $(In_xGa_{1-x})_2O_3$ to the binary III-nitride compounds GaN, AlN, and InN. This methodology might potentially be extended to generalize band offset calculations between heterojunctions of ternary nitrides, ternary oxides, or ternary oxide-nitride superlattices. This task is beyond the scope of this current work, primarily because additional understanding of the effects of strain, polarization, phase segregation, and interfacial defects must be developed, both experimentally and from first principles, in order to identify and minimize potential sources of error. We expect that future heterogeneous integration effort might benefit from integrating such dissimilar materials in order to meet the challenges of next-generation ultra-wide bandgap semiconductor electronic devices.

The project or effort depicted was partially sponsored by the Department of the Defense, Defense Threat Reduction Agency, No. HDTRA1-17-1-011, monitored by Jacob Calkins. The content of the information does not necessarily reflect the position or the policy of the federal government, and no official endorsement should be inferred. Research at the Naval Research Laboratory was supported by the Office of Naval Research.

DATA AVAILABILITY

The data that support the findings of this study are available from the corresponding author upon reasonable request.

REFERENCES

[1]J. Y. Tsao, S. Chowdhury, M. A. Hollis, D. Jena, N. M. Johnson, K. A. Jones, R. J. Kaplar, S. Rajan, C. G. Van de Walle, E. Bellotti, C. L. Chua, R. Collazo, M. E. Coltrin, J. A. Cooper, K. R. Evans, S. Graham, T. A. Grotjohn, E. R. Heller, M. Higashiwaki, M. S. Islam, P. W. Juodawlkis, M. A. Khan, A. D. Koehler, J. H. Leach, U. K. Mishra, R. J. Nemanich, R. C. N. Pilawa-Podgurski, J. B. Shealy, Z. Sitar, M. J. Tadjer, A. F. Witulski, M. Wraback, and J. A. Simmons, Adv. Electron. Mater. **4**, 1600501 (2018).
[2]S. J. Pearton, J. Yang, P. H. Cary, I. V. F. Ren, J. Kim, M. J. Tadjer, and M. A. Mastro, Appl. Phys. Rev. **5**, 011301 (2018).
[3]B. J. Baliga, Semicond. Sci. Technol. **28**, 074011 (2013).
[4]S. Krishnamoorthy, Z. Xia, S. Bajaj, M. Brenner, and S. Rajan, Appl. Phys. Express **10**, 051102 (2017).
[5]U. K. Mishra, P. Parikh, and Y.-F. Wu, "AlGaN/GaN HEMTs-an overview of device operation and applications," Proc. IEEE **90**(6), 1022–1031 (2002).
[6]H. Peelaers, J. B. Varley, J. S. Speck, and C. G. Van de Walle, Appl. Phys. Lett. **112**, 242101 (2018).
[7]R. H. French, J. Am. Ceram. Soc. **13**, 471 (1990).
[8]L. Chen and B. J. Skromme, Appl. Phys. Lett. **85**, 4334 (2004).
[9]N. Nepal, S. B. Qadri, J. K. Hite, N. A. Mahadik, M. A. Mastro, and C. R. Eddy, Jr., Appl. Phys. Lett. **103**, 082110 (2013).
[10]H. Okumura, S. Suihkonen, J. Lemettinen, A. Uedono, Y. Zhang, D. Piedra, and T. Palacios, Jpn. J. Appl. Phys., Part 1 **57**, 04FR11 (2018).
[11]T. Kinoshita, T. Nagashima, T. Obata, S. Takashima, R. Yamamoto, R. Togashi, Y. Kumagai, R. Schlesser, R. Collazo, A. Koukitu, and Z. Sitar, Appl. Phys. Express **8**, 061003 (2015).
[12]Y. Taniyasu, M. Kasu1, and T. Makimoto, Nature **441**, 325 (2006).
[13]M. H. Breckenridge, Q. Guo, A. Klump, B. Sarkar, Y. Guan, J. Tweedie, R. Kirste, S. Mita, P. Reddy, R. Collazo, and Z. Sitar, Appl. Phys. Lett. **116**, 172103 (2020).
[14]R. Yamamoto, N. Takekawa, K. Goto, T. Nagashima, R. Dalmau, R. Schlesser, H. Murakami, R. Collazo, B. Monemar, Z. Sitar, and Y. Kumagai, J. Cryst. Growth **545**, 125730 (2020).
[15]S. Washiyama, P. Reddy, B. Sarkar, M. H. Breckenridge, Q. Guo, P. Bagheri, A. Klump, R. Kirste, J. Tweedie, S. Mita, Z. Sitar, and R. Collazo, J. Appl. Phys. **127**, 105702 (2020).
[16]P. Bagheri, R. Kirste, P. Reddy, S. Washiyama, S. Mita, B. Sarkar, R. Collazo, and Z. Sitar, Appl. Phys. Lett. **116**, 222102 (2020).
[17]M. R. Hauwiller, D. Stowe, T. B. Eldred, S. Mita, R. Collazo, Z. Sitar, and J. LeBeau, APL Mater. **8**, 091110 (2020).
[18]H. Ünlü and A. Asenov, J. Phys. D: Appl. Phys. **35**, 591 (2002).
[19]H. Sun, C. G. Torres Castanedo, K. Liu, K.-H. Li, W. Guo, R. Lin, X. Liu, J. Li, and X. Li, Appl. Phys. Lett. **111**, 162105 (2017).
[20]W. Wei, Z. Qin, S. Fan, Z. Li, K. Shi, Q. Zhu, and G. Z. Wei, Nanoscale Res. Lett. **7**, 562 (2012).
[21]C. Fares, M. J. Tadjer, J. Woodward, N. Nepal, M. A. Mastro, C. R. Eddy, Jr., F. Ren, and S. J. Pearton, ECS J. Solid State Sci. Technol. **8**, Q3154 (2019).
[22]T. L. Duan, J. S. Pan, and D. S. Ang, Appl. Phys. Lett. **102**, 201604 (2013).
[23]A. Eisenhardt, G. Eichapfel, M. Himmerlich, A. Knübel, T. Passow, C. Wang, F. Benkhelifa, R. Aidam, and S. Krischok, Phys. Status Solidi C **9**(3–4), 685 (2012).
[24]H. P. Song, A. L. Yang, H. Y. Wei1, Y. Guo1, B. Zhang1, G. L. Zheng, S. Y. Yang, X. L. Liu, Q. S. Zhu, Z. G. Wang, T. Y. Yang, and H. H. Wang, Appl. Phys. Lett. **94**, 222114 (2009).
[25]C. Fares, F. Ren, E. Lambers, D. C. Hays, B. P. Gila, and S. J. Pearton, J. Electr. Mater. **48**, 1568 (2019).
[26]C. Fares, M. Xian, D. J. Smith, M. R. McCartney, M. Kneiß, H. von Wenckstern, M. Grundmann, M. Tadjer, F. Ren, and S. J. Pearton, J. Appl. Phys. **127**, 105701 (2020).
[27]A. D. Koehler, N. Nepal, T. J. Anderson, M. J. Tadjer, K. D. Hobart, C. R. Eddy, and F. J. Kub, IEEE Electron Dev. Lett. **34**, 1115 (2013).
[28]P. Carey, F. Ren, D. C. Hays, B. P. Gila, S. J. Pearton, S. Jang, and A. Kuramata, Jpn. J. Appl. Phys., Part 1 **56**, 071101 (2017).
[29]E. A. Kraut, R. W. Grant, J. R. Waldrop, and S. P. Kowalczyk, Phys. Rev. Lett. **44**, 1620 (1980).
[30]H. C. Shin, D. Tahir, S. Seo, Y. R. Denny, S. K. Oh, H. J. Kang, S. Heo, J. G. Chung, J. C. Lee, and S. Tougaard, Surf. Interface Anal. **44**, 623 (2012).
[31]E. O. Filatova and A. S. Konashuk, J. Phys. Chem. C **119**, 20755–20761 (2015).
[32]A. Balzarotti and A. Bianconi, Phys. Status Solidi B **76**, 689 (1976).
[33]V. V. Afanas'ev, M. Houssa, A. Stesmans, C. Merckling, T. Schram, and J. A. Kitt, Appl. Phys. Lett. **99**, 072103 (2011).
[34]X.-Y. Cui, S. P. Ringer, G. Wang, and Z. H. Stachurski, J. Chem. Phys. **151**, 194506 (2019).
[35]V. A. Pustovarov, V. Sh. Aliev, T. V. Perevalov, V. A. Gritsenko, and A. P. Eliseev, J. Exp. Theor. Phys. **111**, 989–995 (2010).
[36]T. V. Perevalov, V. A. Gritsenko, and V. V. Kaichev, Eur. Phys. J. Appl. Phys. **52**, 30501 (2010).
[37]I. Costina and R. Franchy, Appl. Phys. Lett. **78**, 4139 (2001).
[38]D. Liu, S. J. Clark, and J. Robertson, Appl. Phys. Lett. **96**, 032905 (2010).
[39]J. Robertson and B. Falabretti, J. Appl. Phys. **100**, 014111 (2006).
[40]A. F. M. Anhar Uddin Bhuiyan, Z. Feng, J. M. Johnson, H.-L. Huang, J. Sarker, M. Zhu, M. R. Karim, B. Mazumder, J. Hwang, and H. Zhao, APL Mater. **8**, 031104 (2020).
[41]E. A. Anber, D. Foley, A. C. Lang, J. Nathaniel, J. L. Hart, M. J. Tadjer, K. D. Hobart, S. J. Pearton, and M. Taheri, Appl. Phys. Lett. **117**, 152101 (2020).